Chemical Science

ROYAL SOCIETY OF CHEMISTRY

EDGE ARTICLE

View Article Online
View Journal | View Issue

Cite this: *Chem. Sci.*, 2020, **11**, 4239

All publication charges for this article have been paid for by the Royal Society of Chemistry

Received 20th December 2019
Accepted 1st April 2020

DOI: 10.1039/c9sc06481h

rsc.li/chemical-science

Visible-light photooxidation in water by $^1O_2$-generating supramolecular hydrogels†

Sankarsan Biswas, [abc] Mohit Kumar, [ab] Andrew M. Levine, [abc] Ian Jimenez,[ae] Rein V. Ulijn *[abcd] and Adam B. Braunschweig *[abcd]

We report supramolecular photocatalytic hydrogels, produced by the enzymatically driven self-assembly of low molecular weight gelators (LMWGs). These LMWG precursors are composed of the organic chromophore diketopyrrolopyrrole (DPP), which is bi-functionalized with a series of amino acid (Phe, Tyr, Leu) methyl esters. *In situ* enzymatic hydrolysis of these photoactive precursors results in supramolecular hydrogels that provide a high density of photocatalytic sites. Under visible light irradiation these hydrophobic fibers recruit the reaction substrates and also produce $^1O_2$, which is used here for the photooxidation of thioanisole (aromatic substrate) and cyclohexyl methyl sulfide (aliphatic substrate), with yields as high as 100% and without over-oxidation. Finally, we demonstrate that the nature of the amino acids in the LWMGs has a central role in dictating J-/H-/mixed state aggregates, gel properties, and, hence, the efficiency of chemoselective photooxidation of thioanisole and cyclohexyl methyl sulfide inside these hydrogels.

Introduction

There is a growing need for new catalytic methods that proceed photochemically under visible light illumination, are compatible with aqueous solvents, and avoid the need for expensive heavy metals, thereby reducing detrimental environmental impacts.[1–9] In this context, organic photocatalysts that operate in aqueous solvents have been the focus of considerable recent interest as sustainable alternatives to conventional photocatalysts.[10–14] To date, these photocatalysts/photosensitizers are primarily porphyrin-based, and their photocatalytic applications are mostly limited to water-soluble substrates.

There remain several substantial challenges that have precluded the broader adoption of aqueous photocatalysts, including their inability to act upon hydrophobic molecules in aqueous media and the lack of alternatives to porphyrin-based photocatalytic systems that work efficiently in water. Catalytic supramolecular hydrogels provide a promising solution to this challenge.[15–19] Hydrogel networks can address the solubility problem because hydrophobic aromatic compounds often associate into the nanofiber network in water and become reactively accessible.[20] For example, the Meijer[21] and Escuder[22] groups have shown that a self-assembled, 1D fiber network enhances catalytic activity compared to its non-assembled counterpart.[23–28] Most recent examples of hydrogel photocatalysts[29] involve co-assembling of the photocatalysts with gelators, where catalysts and gelators are two separate components. These hydrogel photocatalysts were used for the oxidation of iodide,[30] hydrogen production,[31] polymer crosslinking,[32] and artificial photosynthesis.[33,34] There remain, however, several drawbacks with hydrogel photocatalysts, including the limited control of positioning and accessibility of photoactive sites and the possibility of dissociation of non-covalently bound photoactive sites from the gel. We propose that by making the catalyst an integral and inseparable component of the gelator itself, supramolecular photocatalysts could be produced with increased number of photoactive sites and enhanced stability.

Here, we report a new approach to aqueous photocatalysis composed of organic chromophores that assemble into chiral supramolecular hydrogels, where the catalytic site is itself both a structural and functional component of the photoactive gel. The assembly of the gels is driven by aromatic amino acid bola-amphiphiles[35] that form in a controlled manner through biocatalytic self-assembly that occurs following hydrolysis of methyl esters in the presence of α-chymotrypsin.[36,37] This versatile and reproducible biocatalytic assembly approach previously provided functional hydrogels by avoiding productive kinetic aggregates, and is especially relevant to self-

[a]*Advanced Science Research Center, Graduate Center, City University of New York, 85 St. Nicholas Terrace, New York, NY 10031, USA. E-mail: abraunschweig@gc.cuny.edu*

[b]*Department of Chemistry, Hunter College, 695 Park Avenue, New York, NY 10065, USA*

[c]*PhD Program in Chemistry, Graduate Center, City University of New York, New York, NY 10016, USA*

[d]*PhD Program in Biochemistry, Graduate Center, City University of New York, New York, NY 10016, USA*

[e]*The High School for Math, Science, and Engineering, The City College of New York, 240 Convent Avenue, New York, NY 10031, USA*

† Electronic supplementary information (ESI) available: Experimental details, organic synthesis, NMR, MS, TEM, AFM, HPLC, UV-Vis, fluorescence emission spectroscopy and $^1O_2$ calculations. See DOI: 10.1039/c9sc06481h

assembly involving poorly soluble functional components.[38,39] Here, the precursors for these low molecular weight gelators (LMWGs) are composed of the chromophore diketopyrrolopyrrole (DPP) with amino acid methyl esters connected through a linker appended to the heterocyclic N (Fig. 1). The self-assembly is activated *in situ* through enzymatic ester hydrolysis leading to rebalancing of amphiphilicity to favor unidirectional assembly. Aromatic components provide hydrophobic contacts and π···π interactions, and the amino acid residues provide chirality and H-bonding, leading to the formation of 1D superstructures in water. The ability to vary the amino acid side chain provides a versatile route to explore different superstructures.[40] DPP was chosen as the chromophore as it has been used previously to generate $^1O_2$ upon irradiation with visible light,[41–45] which is a powerful oxidizing agent in catalysis.[46–48]

Here we demonstrate the utility of this catalytic platform by oxidizing thioanisole and cyclohexyl methyl sulfide to their corresponding sulfoxides in water, which is a relevant model system because sulfoxides are precursors in the synthesis of several pharmaceuticals and many common preparations suffer from overoxidation to the sulfone.[46,49] We have assessed the catalytic activities of three such DPP-based supramolecular hydrogels that vary in their amino acid side chains, where they include either tyrosine (**Y**), phenylalanine (**F**) or leucine (**L**). The two aromatic amino acids were chosen as they are prone to supramolecular gelation,[50] and aliphatic leucine (**L**) was selected as a control because it forms fibers but is not prone to gelation. We found that the hydrogel state plays a vital role in facilitating catalysis, presumably by sequestering the hydrophobic thioanisole and cyclohexyl methyl sulfide inside the fiber networks. This study demonstrates how the incorporation of photocatalysts in conjunction with hydrogel formation can play a vital role in photooxidation of hydrophobic substrates in water, towards sustainable and environmentally benign visible-light photocatalysis.

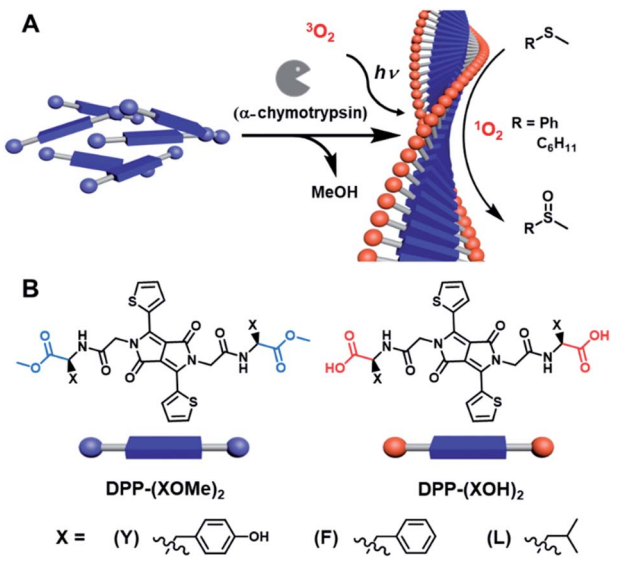

Fig. 1 Visible-light photooxidation enabled by a supramolecular hydrogel. (A) Biocatalytic self-assembly of the LMWGs into superstructures *via in situ* enzymatic hydrolysis of DPP-$(XOMe)_2$ with α-chymotrypsin. These superstructures were used for the photooxidation of thioanisole and cyclohexyl methyl sulfide *via* $^1O_2$ formation in water. (B) Photoactive precursors, DPP-$(XOMe)_2$ and components, DPP-$(XOH)_2$, of the supramolecular hydrogels.

Results and discussion

The design of our LMWGs requires a chromophore that would produce long-lived triplets in response to light, which can generate $^1O_2$, and to which amino acids could be readily appended to direct subsequent aqueous supramolecular assembly. Achieving controlled photooxidation by using dissolved oxygen in aqueous media poses a number of significant challenges because of the low solubility and short $^1O_2$ lifetime.[51,52] Photosensitizers with long excited state lifetimes facilitate efficient energy transfer, converting $^3O_2$ into $^1O_2$, thereby increasing catalytic efficiency. DPP was selected as the photosensitizer because it has been shown previously to generate $^1O_2$ in the context of photodynamic therapy.[45] It is also known that triplet lifetimes for DPP increase from ps[53] to μs[54] upon assembly because the excited state of DPP has the ability to undergo singlet fission. Although, DPP has been used in the context of organic semiconductors and solar cells,[55,56] to our knowledge it has not yet been used for aqueous catalysis or photocatalysis.

All three DPP-$(XOMe)_2$ derivatives were synthesized in four steps following identical procedures. First, the DPP core was prepared by Dieckmann condensation of dimethyl succinate and thiophene-2-carbonitrile with 87% yield. The core was then functionalized at the heterocyclic N with *tert*-butyl acetate *via* an S_N2 substitution with 47% yield. The diester was then hydrolyzed with trifluoroacetic acid in 97% yield, and the final diacid was then functionalized with different amino acids *via* HBTU coupling in 81% yield for DPP-$(YOMe)_2$ (**1Y**), 84% yield for DPP-$(FOMe)_2$ (**1F**), and 81% yield for DPP-$(LOMe)_2$ (**1L**). L-Enantiomers of the amino acids were incorporated to facilitate subsequent α-chymotrypsin catalysed hydrolysis. All LMWG precousors were characterized by ^1H NMR and ^{13}C NMR spectroscopy, and high-resolution mass spectrometry, and all data were consistent with the proposed structures.

Changing amino acids provided access to distinct supramolecular structures for investigating how subtle changes in assembly affect the photophysical properties and catalytic performance of the hydrogels. The assembly was studied by high performance liquid chromatography (HPLC), UV-Vis, fluorescence, and circular dichroism (CD) spectroscopies, transmission electron microscopy (TEM), atomic force microscopy (AFM), and rheology. The DPP heterocycle is hydrophobic and insoluble in most organic and aqueous solvents, and, consequently, the DPP-$(XOMe)_2$ derivatives have limited solubility in aqueous solvents. Thus to make the hydrogels, 200 mM stock solutions of LMWGs **1Y** and **1L** were prepared in DMSO and then diluted with 100 mM phosphate buffer (pH 8) containing 1 mg mL^{-1} α-chymotrypsin (Sigma, lyophilized power, ≥40 units per mg protein). **1F** was sparingly soluble in DMSO at room temperature, so rather than creating a stock solution, it

was directly weighed in a vial and DMSO was added followed by heating until solubilized to create a gel. To this hot DMSO solution, phosphate buffer was added and the solution was sonicated. After the solution reached room temperature, enzyme in phosphate buffer was added to a final concentration of 1 mg mL^{-1}. 10 mM solutions of DPP-$(YOH)_2$ (**3Y**) and DPP-$(FOH)_2$ (**3F**) formed self-supporting hydrogels after 1 h for **3Y** and 2 h for **3F**, while the DPP-$(LOH)_2$ (**3L**) did not gel. All enzymatic hydrolysis reactions were monitored by HPLC to assess the reaction kinetics and yields. The hydrolysis of **1Y** took 7 h to complete (confirmed by LC-MS, Fig. 2C and S16†), whereas **3L** and **1F** took three days for complete hydrolysis, suggesting that gelation occurs well before hydrolysis is completed (Fig. S17 and S18†).

Because of its faster hydrolysis and gelation, **1Y** was used to explore the kinetics and photophysical properties of gelation in greater detail. As **3Y** formed a self-supporting gel at 10 mM, the characterization studies were performed at this concentration, unless otherwise noted. We first used HPLC to monitor the kinetics of enzymatic hydrolysis. After exposing **1Y** to the enzyme, aliquots of the reaction mixtures were taken periodically and added to a 1 : 1 CH_3CN : H_2O mixture for HPLC-MS analysis. All species present in the enzymatic reaction were characterized by high-resolution mass spectroscopy, which, together with HPLC chromatograms, confirmed the presence of **1Y**, MeOY-DPP-YOH (**2Y**) and **3Y** in the reaction mixtures. The relative peak integrations showed an increase of **3Y** with a decay of **1Y** over time (Fig. 2C). The intermediate **2Y** was observed within the first 8 min of the reaction, after which **3Y** became the dominating species in the reaction mixture. It was found that 92% conversion into **3Y** was observed within 3 h, while complete hydrolysis (>96%) took 7 h. Superstructure formation during hydrolysis was monitored by CD spectroscopy. After exposing **1Y** to the enzyme, aliquots of the reaction mixtures were taken periodically for CD measurements. A bisignated CD signal was observed with a positive signal from 650 nm to 550 nm followed by a negative signal from 550 nm to 450 nm (Fig. 2D), and signal intensity increased for all peaks over time.

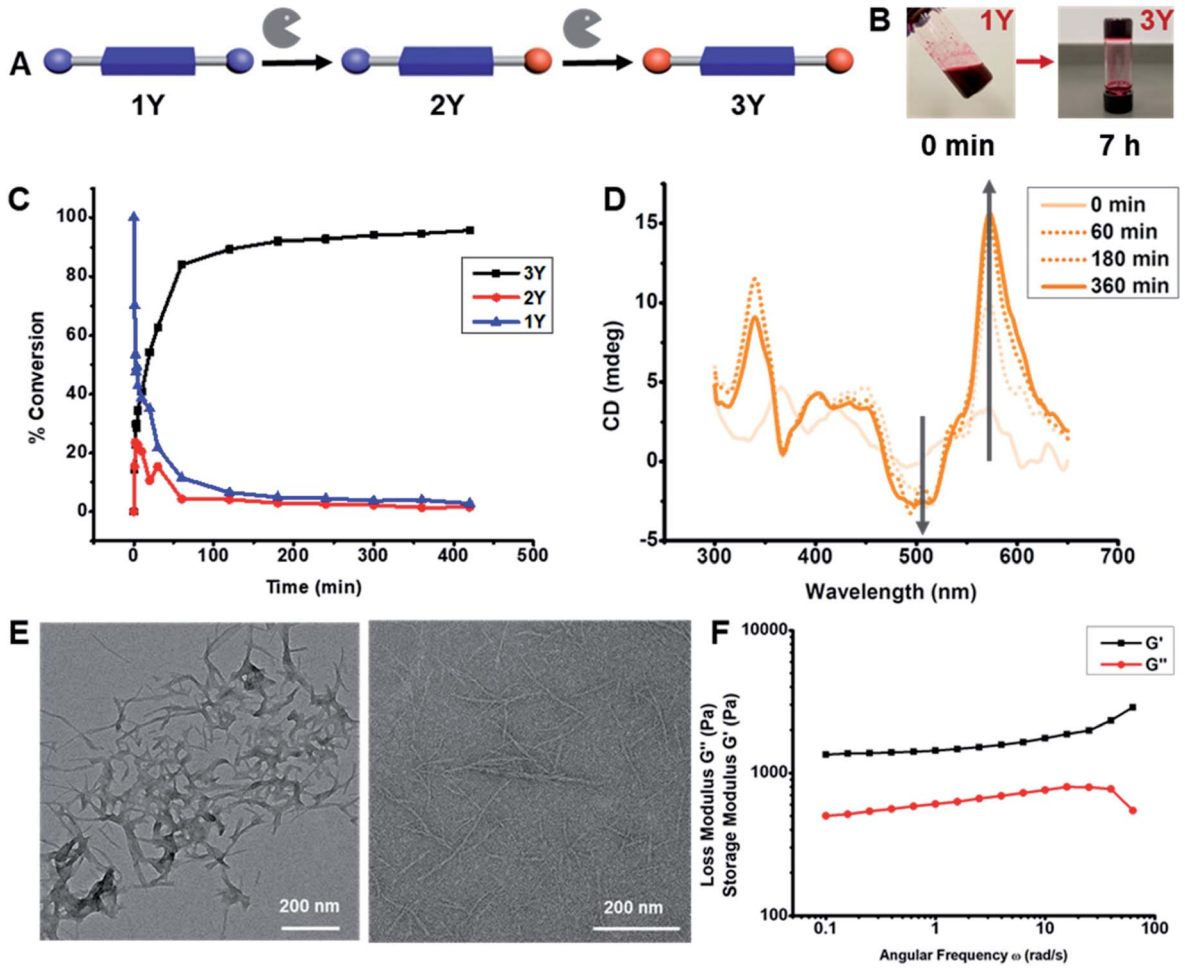

Fig. 2 (A) Enzymatic hydrolysis of DPP-$(YOMe)_2$ in phosphate buffer (pH 8, 100 mM, 5% DMSO) in the presence of α-chymotrypsin (1 mg mL^{-1}). (B) Photograph of reaction vial at 0 min (left) and at 7 h (right). (C) HPLC analysis of enzymatic hydrolysis of DPP-$(YOMe)_2$ at 10 mM. (D) CD spectra showing the formation of homochiral superstructure during the enzymatic hydrolysis of DPP-$(YOMe)_2$ at 10 mM. (E) TEM images of DPP-$(YOMe)_2$ (left) and DPP-$(YOH)_2$ (right). (F) Oscillatory rheology of the DPP-$(YOH)_2$ (10 mM) gel showing elastic modulus (G') of 1.7 kPa (angular frequency = 10 rad s^{-1}; frequency sweep).

This bisignated cotton effect is a hallmark of dyes that are aggregated into homochiral helical superstructures.[57,58] Signal intensity approached saturation after 3 h, when HPLC data suggests that 92% of the hydrolysis is completed. Similarly, aliquots of the reaction mixtures of **3F** and **3L** were analyzed by CD after 3 d of exposure to α-chymotrypsin. When comparing CD spectra for DPP-$(XOH)_2$, it was found that **3L** and **3Y** have similar bisignated CD signals between 650–450 nm, whereas the CD signal of **3F** had a negative signal from 650 nm to 560 nm followed by a positive signal from 560 nm to 525 nm (Fig. S20†). The different CD signal for **3F**, confirms that superstructure geometry is dependent upon **F**, **Y**, **L** amino acid side chains.

The biocatalytic self-assembly of **1Y** was also monitored by UV-Vis (Fig. S21†) and fluorescence (Fig. S22†) spectroscopies to observe the photophysical changes that occurred upon their transformation into 1D-superstructures. To monitor the changes of the UV-Vis spectra over time, the reaction mixture was sonicated and vortexed for 10 s, and aliquots of **1Y** (10 mM in 100 mM phosphate buffer pH 8 with 5% DMSO and 1 mg mL^{-1} enzyme) were periodically analyzed. Time dependent UV-Vis spectroscopy revealed a change in the intensity ratio of the characteristic DPP λ_{max} at 512 nm and 540 nm, corresponding to the 0–1 and 0–0 transitions, respectively (Fig. S21C†). It has been previously reported that H- and J-aggregates can be differentiated for the DPP dyes based upon the ratio of 0–1/0–0 vibronic peaks, where a higher 0–1 peak indicates H-aggregates, and a higher 0–0 peak is suggestive of J-aggregates.[59–61] By monitoring the change in this ratio during hydrolysis it was found that the ratio went from more than unity (t < 40 min) to less than unity (t > 40 min), suggesting that J-aggregates form upon biocatalytic hydrolysis and assembly. Comparative analysis of the UV-Vis spectra (Fig. S21D†) of all DPP-$(XOH)_2$ showed that **3L** has a sharper absorbance and less scattering compared to **3F** and **3Y** which have much broader features and more scattering in the UV-Vis spectrum which could be related to the relative degrees of gelation. The final 0–1/0–0 ratios of all DPP-$(XOH)_2$ are also dependent upon the amino acids. These data suggest that **3L** formed H-aggregates, whereas **3Y** is a J-aggregate, and **3F** is a mixed state. Time dependent fluorescence for the hydrolysis of **1Y** (λ_{ex} = 450 nm, 10 mM) showed that the intensity at 557 nm and 601 nm increased for the first 50 min, after which intensity gradually decreased until 100 min, when hydrolysis is nearly completed (Fig. S22†). Comparison of the fluorescence spectra of all three DPP-$(XOH)_2$, taken after 1 d for **3Y** and 3 d for **3F** and **3L**, showed that **3L** has the highest emission intensity among all DPP-$(XOH)_2$ (Fig. S23†), which can be explained because aggregation of DPP leads to quenching,[62] and the most weakly assembled hydrogel has the least aggregation-induced quenching. **3F**, in contrast showed the least emission intensity, suggesting the formation of a highly aggregated species (Fig. S23†).

Further evidence of superstructure formation was provided by TEM and AFM images of **1Y** (Fig. 2E, S10 and S12†) and **3Y** (Fig. 2E, S11 and S13†) that were taken at 0 min and at 7 h after exposure to the enzyme. AFM and TEM show fibers with 6.2 ± 1 nm diameters. This diameter is larger than that of the molecular dimension of **3Y** (~2 nm) suggesting bundle formation rather than single molecular stacks. Microscopic evidence of fiber formations for **3L** and **3F** were also obtained by TEM imaging. Although **1Y** transformed into uniform fibers after enzymatic hydrolysis, **3L** and **3F** formed a distribution of both thin fibers and bundled fibers (Fig. S14 and S15†). These data confirm that all LMWGs formed 1D-superstructures upon enzymatic hydrolysis, although only **1Y** and **1F** formed hydrogels. Rheology measurements on **3Y** and **3F** were performed to define viscoelastic moduli and it was found that **3Y** has an elastic moduli (G') of 1.7 kPa (angular frequency = 10 rad s^{-1}) in the frequency sweep (Fig. 2F). Rheology measurements on **3F** showed the formation of a much stronger hydrogel (G' of 21 kPa; angular frequency = 10 rad s^{-1}) compared to **3Y** (Fig. S26†).

Next, all these DPP-$(XOH)_2$ were then tested for their ability to produce $^1O_2$ upon photoirradiation. $^1O_2$ yields for these DPP-$(XOH)_2$ catalysts were determined by following a previously reported indirect method, where methylene blue (MB) was used as a standard photosensitizer and 1,3-diphenylisobenzofuran (DPBF) as an indicator.[63] Please note that due to high extinction coefficient of DPP, we were unable to use this method in water at the gelation concentration. All catalysts (**3Y**, **3F**, **3L**) were first dissolved in DMSO, then DPBF and the catalysts were mixed in a 1 : 1 ratio and saturated with air. These mixtures were excited for 2 min (λ_{ex} = 534 nm for **3L**, λ_{ex} = 535 nm for **3Y** and λ_{ex} = 535 nm for **3F**) in a fluorimeter, and absorbance were taken immediately after excitation to monitor changes in DPBF intensity. This process was then repeated 5 more times. The decrease in absorbance at 418 nm from the photooxidation of DPBF by $^1O_2$ was then compared with the decrease caused by MB under identical experimental conditions to provide $^1O_2$ yields of 67% for **3Y** and 71% for **3L**, which is the highest $^1O_2$ yield reported yet for DPP-based molecules,[64] and 47% for **3F** (Fig. S24†).

We then demonstrated the photooxidation of thioanisole and cyclohexyl methyl sulfide by these supramolecular hydrogels. The challenge associated with sulfoxidation in water is that the precursor sulfides are hydrophobic and generally insoluble in water. The nanofiber network of photocatalysts surrounding them could increase substrate accessibility towards the photocatalysts. The oxidation experiments were performed in 1 mL solutions of catalysts prepared in 5 mL vials *via* enzymatic hydrolysis of the corresponding DPP-$(XOMe)_2$. Thioanisole and cyclohexyl methyl sulfide were then added into these systems after 7 h for **3Y** and after 3 d for **3F** and **3L** and stirred under positive pressure of air for 3 days. A white light source (150 W Fiber Optic Dual Gooseneck Microscope Illuminator) was used for all photooxidation reactions. To explore the reaction scope and the effect of reaction conditions on yield, we varied solvent, and the amino acid substitutions chain and concentration of DPP-$(XOH)_2$ (Table 1). For initial optimization of the reaction conditions, we used thioanisole as a model substrate. For **3Y** it was found that yield increases with increasing concentration of supramolecular catalyst, with an increase in yield from 2% to 30% as [**3Y**] increases from 5 mM to 10 mM, and a similar trend was observed upon increasing [**3F**] from 5 mM to 10 mM giving rise to an increase from 14% to 39%. In both cases, gelation was

Table 1 Sulfoxidation of thioanisole and cyclohexyl methyl sulfide by photogenerated $^1O_2$ in the presence of a supramolecular DPP hydrogel with varying LMWGs and solvents (D_2O or H_2O)[a]

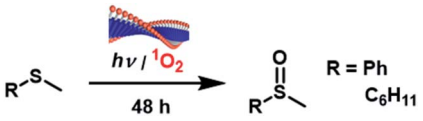

Catalyst	[Catalyst] (mM)	Substrate	Yield (%)
—	0	R = Ph	0
7	10	R = Ph	5
3Y	1	R = Ph	1
3Y	5	R = Ph	2
3Y	10	R = Ph	30
3Y	10 (1 : 1 D_2O/H_2O)	R = Ph	44
3Y	10 (D_2O)	R = Ph	86
3Y	20	R = Ph	6
3Y	30	R = Ph	5
3L	10	R = Ph	10
3F	5	R = Ph	14
3F	10	R = Ph	39
3F	10 (D_2O)	R = Ph	67
1Y	10	R = Ph	9
1Y	20	R = Ph	2
1L	10	R = Ph	5
1F	10	R = Ph	17
3Y	10	R = C_6H_{11}	100
3F	10	R = C_6H_{11}	94
3L	10	R = C_6H_{11}	88

[a] Unless otherwise noted, all reactions were conducted with 1.0 mL of reaction solutions and were used for photooxidation after enzymatic hydrolysis of corresponding DPP-$(XOMe)_2$ without any further purification. Thioanisole and cyclohexyl methyl sulfide were added to these solutions and stirred under positive pressure of air for 48 h. Final concentration of the sulfides were 0.4 mM in the hydrogel. The solution was irradiated with a white halogen light that was connected to the reaction chamber with an optical fiber and reactions were performed at rt. All yields were calculated from HPLC.

only observed at the higher concentration, indicating that gelation and fiber formation have a positive role in catalysis. The observed yield decreased at [**3Y**] > 10 mM, which can be explained by the poor light penetration at higher [**3Y**] as a consequence of the high extinction coefficient of the LMWGs or because of slower diffusion of the reactants through this denser gel. For further confirmation of the positive effect of gelation on catalysis, 10 mM of **3L**, which does not form a hydrogel, was examined as a catalyst for the photooxidation of thioanisole. Under the same reaction conditions, the yield at 10 mM (10%) was much lower compared to the gel-forming samples. In addition, a control experiment with soluble 10 mM DPP-acetate (**7**) was performed which gave rise to a much reduced oxidation yield of 3% compared to that observed in **3Y**, **3F** and **3L**. These observations strongly suggest that both fiber formation and hydrogelation are crucial for the catalysis, presumably because the gel networks trap hydrophobic thioanisole molecules and improve the accessibility towards photoactive sites. All non-assembled/randomly assembled precursors (DPP-$(XOMe)_2$) of these catalysts had lower yields than the assembled forms of these catalysts. Yields were further increased to 87% in **3Y** (10 mM) and 67% in **3F** (10 mM) by using D_2O phosphate buffer as a solvent. It is known that $^1O_2$ has a higher lifetime in D_2O (68 μs) *vs.* H_2O (4 μs).[65] 1 : 1 (v/v) mixture of D_2O and H_2O had half the yield (44%) compared to catalysis in 100% D_2O. Photooxidation experiments in D_2O were only performed for **3Y** and **3F** as these catalysts gave higher yields in H_2O compared to **3L**. In order to investigate if the higher yields for **3Y** and **3F** are related to the interaction of the substrate with aromatic cores of **F**/**Y** and thioanisole, we have carried out our photooxidation reaction with cyclohexyl methyl sulfide (aliphatic sulfide) with all three catalysts. These experiments resulted in photooxidation yields of 100%, 94%, and 88% for **3Y**, **3F**, and **3L** respectively. This suggests that **3Y** is a better catalyst than **3L** for non-aromatic substrates as well, thus suggesting that hydrogelation, or more precisely, the favorable fiber/solvent interactions may indeed have a positive effect in catalysis, although the differences are more pronounced for aromatic substrates. The overall higher yield is not surprising as a similar trend has been reported previously for enantioselective sulfoxidation using a series of flavin–cyclodextrin conjugates of both aromatic and aliphatic suflides.[66] To further confirm that this reaction is indeed photocatalyzed, we performed control experiments both with 10 mM of **3Y** in dark and without any catalyst. Both of these failed to produce sulfoxide. Another control experiment for the photooxidation of thioanisole, using agarose hydrogel (5 mg mL^{-1}), containing soluble DPP-acetate, **7** (see ESI†), was performed. This experiment resulted in 5% yield of the oxidized product, which is significantly lower than that of self-assembled DPP-hydrogelator photocatalysts. We believe that this experiment clearly suggests the advantages of hydrogelators, where the photocatalyst is itself an integral and inseparable component of the gelator. In addition, we found that the photooxidation proceeds optimally at room temperature with 2.5 mol% catalyst loading. Finally, the absence of any evidence of sulfone in HPLC data showed that this approach is also chemoselective and does not suffer from over oxidation.[67–70]

Conclusions

A new strategy for photooxidation that combines supramolecular gelation and catalysis in an effort to simultaneously achieve high yield, circumvent the need for toxic and expensive metals, and operate in water has been studied. A small library of supramolecular catalysts was obtained by varying amino acids appended to the heterocyclic N of the DPP core. Tuning the hydrophobicity of the amino acids enabled us to access different superstructures (H-/J-/mixed state) and photophysical properties. In studying the conditions for the catalytic photooxidation of thioanisole and cyclohexyl methyl sulfide in water, it was found that the favorable solvent/fiber interactions that cause hydrogelation, and supramolecular aggregation of the photocatalyst play a vital role in catalytic efficacy. The effect is more prominent in the case of aromatic substrates. Lower yields for the oxidation of thioanisole in H_2O compared to D_2O can be

explained by the relative low $^1O_2$ lifetimes in the former. This catalyst is designed following the principles of hierarchical structure and emergent photophysics that are common in nature, but not yet widely adopted by the catalytic community, and this manuscript shows how at least some of the major challenges in synthesis could be addressed by this approach.[71] Finally, the high $^1O_2$ yield in these DPP hydrogels and our design approach have potential further applications towards sustainable asymmetric visible-light photocatalysis, wastewater remediation, oxygen sensing, and photodynamic therapy.

Conflicts of interest

There are no conflicts to declare.

Acknowledgements

We thank the Air Force Office of Scientific Research (FA9550-19-1-0220), National Science Foundation (NSF) grant number CHE-1808143, CHE-1G10755, and CHE-2003847. National Science Foundation CREST Center for Interface Design and Engineered Assembly of Low Dimensional Systems (IDEALS), NSF grant number HRD-1547830. The NMR data (Bruker Avance 300 MHz) presented herein were collected in part at the CUNY ASRC Biomolecular NMR facility and the NMR facility of the City College of the CUNY. Mass spectra were collected at the CUNY ASRC Biomolecular Mass Spectrometry Facility and the Hunter College Mass Spectrometry Facility of the CUNY. We thank Dr Barney Yoo (Hunter College Mass Spectrometry Facility) for help in acquiring the spectral data and Dhwanit R. Dave for rheology measurements.

Notes and references

1 C. Ayed, L. Caire da Silva, D. Wang and K. A. I. Zhang, *J. Mater. Chem. A*, 2018, **6**, 22145–22151.
2 J. Byun, W. Huang, D. Wang, R. Li and K. A. I. Zhang, *Angew. Chem., Int. Ed.*, 2018, **57**, 2967–2971.
3 S. Ghasimi, S. Prescher, Z. J. Wang, K. Landfester, J. Yuan and K. A. Zhang, *Angew. Chem., Int. Ed. Engl.*, 2015, **54**, 14549–14553.
4 W. Huang, Z. J. Wang, B. C. Ma, S. Ghasimi, D. Gehrig, F. Laquai, K. Landfester and K. A. I. Zhang, *J. Mater. Chem. A*, 2016, **4**, 7555–7559.
5 J. Liu and M. Antonietti, *Energy Environ. Sci.*, 2013, **6**, 1486–1493.
6 B. Long, Z. Ding and X. Wang, *ChemSusChem*, 2013, **6**, 2074–2078.
7 M. Mitsunaga, M. Ogawa, N. Kosaka, L. T. Rosenblum, P. L. Choyke and H. Kobayashi, *Nat. Med.*, 2011, **17**, 1685.
8 K. T. Oppelt, J. Gasiorowski, D. A. M. Egbe, J. P. Kollender, M. Himmelsbach, A. W. Hassel, N. S. Sariciftci and G. Knör, *J. Am. Chem. Soc.*, 2014, **136**, 12721–12729.
9 H. Urakami, K. Zhang and F. Vilela, *Chem. Commun.*, 2013, **49**, 2353–2355.
10 H.-Y. Xie, L.-S. Han, S. Huang, X. Lei, Y. Cheng, W. Zhao, H. Sun, X. Wen and Q.-L. Xu, *J. Org. Chem.*, 2017, **82**, 5236–5241.
11 W. Chen, F. N. Rein and R. C. Rocha, *Angew. Chem., Int. Ed.*, 2009, **48**, 9672–9675.
12 S. Fukuzumi, T. Kishi, H. Kotani, Y.-M. Lee and W. Nam, *Nat. Chem.*, 2011, **3**, 38–41.
13 M. Gryszel, R. Rybakiewicz and E. D. Głowacki, *Adv. Sustainable Syst.*, 2019, **3**, 1900027.
14 T. Ishizuka, S. Ohkawa, H. Ochiai, M. Hashimoto, K. Ohkubo, H. Kotani, M. Sadakane, S. Fukuzumi and T. Kojima, *Green Chem.*, 2018, **20**, 1975–1980.
15 Q. Fu, C. Duan, Z. Yan, Y. Li, Y. Si, L. Liu, J. Yu and B. Ding, *Macromol. Rapid Commun.*, 2018, **39**, 1800058.
16 W. Jiang, Y. Zhu, G. Zhu, Z. Zhang, X. Chen and W. Yao, *J. Mater. Chem. A*, 2017, **5**, 5661–5679.
17 F. Zhao, J. Bae, X. Zhou, Y. Guo and G. Yu, *Adv. Mater.*, 2018, **30**, 1801796.
18 M. C. Nolan, J. J. Walsh, L. L. E. Mears, E. R. Draper, M. Wallace, M. Barrow, B. Dietrich, S. M. King, A. J. Cowan and D. J. Adams, *J. Mater. Chem. A*, 2017, **5**, 7555–7563.
19 J. Byun, K. Landfester and K. A. I. Zhang, *Chem. Mater.*, 2019, **31**, 3381–3387.
20 N. Singh, M. P. Conte, R. V. Ulijn, J. F. Miravet and B. Escuder, *Chem. Commun.*, 2015, **51**, 13213–13216.
21 L. N. Neumann, M. B. Baker, C. M. A. Leenders, I. K. Voets, R. P. M. Lafleur, A. R. A. Palmans and E. W. Meijer, *Org. Biomol. Chem.*, 2015, **13**, 7711–7719.
22 M. Tena-Solsona, J. Nanda, S. Díaz-Oltra, A. Chotera, G. Ashkenasy and B. Escuder, *Chem.–Eur. J.*, 2016, **22**, 6687–6694.
23 N. J. Hestand, R. V. Kazantsev, A. S. Weingarten, L. C. Palmer, S. I. Stupp and F. C. Spano, *J. Am. Chem. Soc.*, 2016, **138**, 11762–11774.
24 A. S. Weingarten, R. V. Kazantsev, L. C. Palmer, D. J. Fairfield, A. R. Koltonow and S. I. Stupp, *J. Am. Chem. Soc.*, 2015, **137**, 15241–15246.
25 O. Zozulia, M. A. Dolan and I. V. Korendovych, *Chem. Soc. Rev.*, 2018, **47**, 3621–3639.
26 C. Zhang, X. Xue, Q. Luo, Y. Li, K. Yang, X. Zhuang, Y. Jiang, J. Zhang, J. Liu, G. Zou and X.-J. Liang, *ACS Nano*, 2014, **8**, 11715–11723.
27 K. Tao, B. Xue, S. Frere, I. Slutsky, Y. Cao, W. Wang and E. Gazit, *Chem. Mater.*, 2017, **29**, 4454–4460.
28 P. Makam, S. S. R. K. C. Yamijala, K. Tao, L. J. W. Shimon, D. S. Eisenberg, M. R. Sawaya, B. M. Wong and E. Gazit, *Nat. Catal.*, 2019, **2**, 977–985.
29 B. Sun, K. Tao, Y. Jia, X. Yan, Q. Zou, E. Gazit and J. Li, *Chem. Soc. Rev.*, 2019, **48**, 4387–4400.
30 S. Frühbeißer, G. Mariani and F. Gröhn, *Polymers*, 2016, **8**, 180.
31 J. Sun, B. V. K. J. Schmidt, X. Wang and M. Shalom, *ACS Appl. Mater. Interfaces*, 2017, **9**, 2029–2034.
32 J. Liu, T. An, Z. Chen, Z. Wang, H. Zhou, T. Fan, D. Zhang and M. Antonietti, *ACS Appl. Mater. Interfaces*, 2017, **5**, 8933–8938.

33 K. Liu, X. Ren, J. Sun, Q. Zou and X. Yan, *Adv. Sci.*, 2018, **5**, 1701001.
34 J. H. Kim, M. Lee, J. S. Lee and C. B. Park, *Angew. Chem., Int. Ed.*, 2012, **51**, 517–520.
35 J. Raeburn, A. Zamith Cardoso and D. J. Adams, *Chem. Soc. Rev.*, 2013, **42**, 5143–5156.
36 Z. Feng, T. Zhang, H. Wang and B. Xu, *Chem. Soc. Rev.*, 2017, **46**, 6470–6479.
37 S. Fleming and R. V. Ulijn, *Chem. Soc. Rev.*, 2014, **43**, 8150–8177.
38 M. Kumar, N. L. Ing, V. Narang, N. K. Wijerathne, A. I. Hochbaum and R. V. Ulijn, *Nat. Chem.*, 2018, **10**, 696–703.
39 S. K. M. Nalluri, C. Berdugo, N. Javid, P. W. J. M. Frederix and R. V. Ulijn, *Angew. Chem., Int. Ed.*, 2014, **53**, 5882–5887.
40 S. Bai, S. Debnath, N. Javid, P. W. J. M. Frederix, S. Fleming, C. Pappas and R. V. Ulijn, *Langmuir*, 2014, **30**, 7576–7584.
41 X. Liang, Z. Guo, H. Wei, X. Liu, H. Lv and H. Xing, *Chem. Commun.*, 2018, **54**, 13002–13005.
42 Y. Liu, T. Pauloehrl, S. I. Presolski, L. Albertazzi, A. R. A. Palmans and E. W. Meijer, *J. Am. Chem. Soc.*, 2015, **137**, 13096–13105.
43 K. R. Weishaupt, C. J. Gomer and T. J. Dougherty, *Cancer Res.*, 1976, **36**, 2326–2329.
44 X.-F. Zhang and X. Yang, *J. Phys. Chem. B*, 2013, **117**, 5533–5539.
45 Y. Cai, P. Liang, Q. Tang, X. Yang, W. Si, W. Huang, Q. Zhang and X. Dong, *ACS Nano*, 2017, **11**, 1054–1063.
46 R. Bentley, *Chem. Soc. Rev.*, 2005, **34**, 609–624.
47 I. Fernández and N. Khiar, *Chem. Rev.*, 2003, **103**, 3651–3706.
48 J. Han, V. A. Soloshonok, K. D. Klika, J. Drabowicz and A. Wzorek, *Chem. Soc. Rev.*, 2018, **47**, 1307–1350.
49 I. Agranat and H. Caner, *Drug Discovery Today*, 1999, **4**, 313–321.
50 A. Lampel, S. A. McPhee, H.-A. Park, G. G. Scott, S. Humagain, D. R. Hekstra, B. Yoo, P. W. J. M. Frederix, T.-D. Li, R. R. Abzalimov, S. G. Greenbaum, T. Tuttle, C. Hu, C. J. Bettinger and R. V. Ulijn, *Science*, 2017, **356**, 1064–1068.
51 X. Xie, C. Mao, X. Liu, Y. Zhang, Z. Cui, X. Yang, K. W. K. Yeung, H. Pan, P. K. Chu and S. Wu, *ACS Appl. Mater. Interfaces*, 2017, **9**, 26417–26428.
52 M. T. Jarvi, M. J. Niedre, M. S. Patterson and B. C. Wilson, *Photochem. Photobiol.*, 2006, **82**, 1198–1210.
53 C. M. Mauck, P. E. Hartnett, E. A. Margulies, L. Ma, C. E. Miller, G. C. Schatz, T. J. Marks and M. R. Wasielewski, *J. Am. Chem. Soc.*, 2016, **138**, 11749–11761.
54 A. M. Levine, C. Schierl, B. S. Basel, M. Ahmed, B. A. Camargo, D. M. Guldi and A. B. Braunschweig, *J. Phys. Chem. C*, 2019, **123**, 1587–1595.
55 C. X. Guzman, R. M. K. Calderon, Z. Li, S. Yamazaki, S. R. Peurifoy, C. Guo, S. K. Davidowski, M. M. A. Mazza, X. Han, G. Holland, A. M. Scott and A. B. Braunschweig, *J. Phys. Chem. C*, 2015, **119**, 19584–19589.
56 Y. Zhou, C. X. Guzman, L. C. Helguero-Kelley, C. Liu, S. R. Peurifoy, B. Captain and A. B. Braunschweig, *J. Phys. Org. Chem.*, 2016, **29**, 689–699.
57 S. Rieth, Z. Li, C. E. Hinkle, C. X. Guzman, J. J. Lee, S. I. Nehme and A. B. Braunschweig, *J. Phys. Chem. C*, 2013, **117**, 11347–11356.
58 E. Schwartz, V. Palermo, C. E. Finlayson, Y.-S. Huang, M. B. J. Otten, A. Liscio, S. Trapani, I. González-Valls, P. Brocorens, J. J. L. M. Cornelissen, K. Peneva, K. Müllen, F. C. Spano, A. Yartsev, S. Westenhoff, R. H. Friend, D. Beljonne, R. J. M. Nolte, P. Samorì and A. E. Rowan, *Chem.–Eur. J.*, 2009, **15**, 2536–2547.
59 S. Militzer, T. M. P. Tran, P. J. Mésini and A. Ruiz-Carretero, *ChemNanoMat*, 2018, **4**, 790–795.
60 F. C. Spano, *Acc. Chem. Res.*, 2010, **43**, 429–439.
61 M. Más-Montoya and R. A. J. Janssen, *Adv. Funct. Mater.*, 2017, **27**, 1605779.
62 D. Ley, C. X. Guzman, K. H. Adolfsson, A. M. Scott and A. B. Braunschweig, *J. Am. Chem. Soc.*, 2014, **136**, 7809–7812.
63 W. Li, L. Li, H. Xiao, R. Qi, Y. Huang, Z. Xie, X. Jing and H. Zhang, *RSC Adv.*, 2013, **3**, 13417–13421.
64 M. Lan, S. Zhao, W. Liu, C.-S. Lee, W. Zhang and P. Wang, *Adv. Healthcare Mater.*, 2019, **8**, 1900132.
65 M. Bregnhøj, M. Westberg, F. Jensen and P. R. Ogilby, *Phys. Chem. Chem. Phys.*, 2016, **18**, 22946–22961.
66 T. Hartman, V. Herzig, M. Buděšínský, J. Jindřich, R. Cibulka and T. Kraus, *Tetrahedron: Asymmetry*, 2012, **23**, 1571–1583.
67 A. Casado-Sánchez, R. Gómez-Ballesteros, F. Tato, F. J. Soriano, G. Pascual-Coca, S. Cabrera and J. Alemán, *Chem. Commun.*, 2016, **52**, 9137–9140.
68 J. Dad'ová, E. Svobodová, M. Sikorski, B. König and R. Cibulka, *ChemCatChem*, 2012, **4**, 620–623.
69 D. Latassa, O. Enger, C. Thilgen, T. Habicher, H. Offermanns and F. Diederich, *J. Mater. Chem.*, 2002, **12**, 1993–1995.
70 T. Neveselý, E. Svobodová, J. Chudoba, M. Sikorski and R. Cibulka, *Adv. Synth. Catal.*, 2016, **358**, 1654–1663.
71 D. Kroiss, G. Ashkenasy, A. B. Braunschweig, T. Tuttle and R. V. Ulijn, *Chem*, 2019, **5**, 1917–1920.